Field-induced magnetic phases and electric polarization in $LiNiPO_4$

Thomas Bagger Stibius Jensen,[1] Niels Bech Christensen,[1,2] Michel Kenzelmann,[2,3] Henrik Moodysson Rønnow,[2,4] Christof Niedermayer,[2] Niels Hessel Andersen,[1] Kim Lefmann,[1] Jürg Schefer,[2] Martin v. Zimmermann,[5] Jiying Li,[6] Jerel L. Zarestky,[6] and David Vaknin[6]

[1]*Materials Research Division, Risø DTU, Technical University of Denmark, DK-4000 Roskilde, Denmark*

[2]*Laboratory for Neutron Scattering, ETH Zürich and Paul Scherrer Institute, CH-5232 Villigen, Switzerland*

[3]*Laboratory for Solid State Physics, ETH Zürich, CH-8093 Zürich, Switzerland*

[4]*Laboratory for Quantum Magnetism, Ecole Polytechnique Fédérale de Lausanne, CH-1015 Lausanne, Switzerland*

[5]*Hamburger Synchrotronstrahlungslabor, Deutsches Elektronen Synchrotron, 22603 Hamburg, Germany*

[6]*Department of Physics and Astronomy and Ames Laboratory, Iowa State University, Ames, Iowa 50011, USA*

(Received 11 November 2008; published 20 March 2009)

Neutron diffraction is used to probe the (H,T) phase diagram of magnetoelectric (ME) $LiNiPO_4$ for magnetic fields along the c axis. At zero field the Ni spins order in two antiferromagnetic phases. One has commensurate (C) structures and general ordering vectors $\mathbf{k}_C=(0,0,0)$; the other one is incommensurate (IC) with $\mathbf{k}_{IC}=(0,q,0)$. At low temperatures the C order collapses above $\mu_0 H=12$ T and adopts an IC structure with modulation vector parallel to $\mathbf{k}_{IC}$. We show that C order is required for the ME effect and establish how electric polarization results from a field-induced reduction in the total magnetoelastic energy.

DOI: 10.1103/PhysRevB.79.092412 PACS number(s): 75.25.+z, 75.30.Gw, 75.80.+q

Materials with both magnetic and electric orders as found in magnetoelectric (ME) multiferroics have received growing interest in recent years.[1–3] It is expected that the coupling of magnetic and electric orders in multiferroics will be of technological use, but will also lead to rich physics with multiorder phase transitions[4] and excitations such as electromagnons.[5,6] Often ferroelectric and magnetic phases have very different ordering temperatures, suggesting that they are driven by different microscopic interactions, but for some they coincide and ferroelectricity is generated by magnetic long-range order.[7–9] In the lithium orthophosphates, $LiMPO_4$ (M=Mn,Fe,Co,Ni), a strong ME effect is observed in the antiferromagnetic phases. Mercier[10] explained the temperature dependence of the ME coefficients for $LiMnPO_4$ and $LiCoPO_4$ and to lesser extent for $LiFePO_4$ with a microscopic model adapted from Cr_2O_3.[11] However, the ME effect in $LiNiPO_4$ differs from that in the other lithium phosphates and was not modeled as successfully. In the present study we determine the field-induced magnetic structures in $LiNiPO_4$ for fields $\mathbf{H}\|\mathbf{c}$ and correct the existing picture of the zero-field structures. Combining symmetry arguments and microscopic calculations similar to Refs. 11 and 12, we use the detailed information of the magnetic structures to quantify the ME properties of $LiNiPO_4$ and show how magnetic fields may lead to electric polarization.

In $LiNiPO_4$, an electric polarization along the a axis (c axis) is generated when a magnetic field is applied along the c axis (a axis). This occurs below $T=20.8$ K, where at zero field the material undergoes a first-order transition from a low-temperature commensurate (C) antiferromagnetic phase with a general ordering vector $\mathbf{k}_C=(0,0,0)$ for each of the four Ni-spin sublattices [cf. Fig. 1(a)] to an incommensurate (IC) phase with $\mathbf{k}_{IC}=(0,q,0)$ and $0.07<q<0.155$.[13] For fields $\mathbf{H}\|\mathbf{c}$, the magnetization measurements provide evidence for several phase transitions between $\mu_0 H=12$ and 22 T.[14] Also IC magnetic structures have been discussed as a possible explanation of hysteresis observed in the ME coefficients at high magnetic fields along the a axis.[15,16]

To understand the ME effect in $LiNiPO_4$, we have studied the (H,T) phase diagram and the magnetic structures for fields $\mathbf{H}\|\mathbf{c}$ up to $\mu_0 H=14.7$ T. We first present the (H,T) phase diagram and show that off-diagonal single-ion anisotropies and Dzyaloshinsky-Moriya (DM) interactions allowed by symmetry are consistent with the observed magnetic structures and lead to staggered magnetic moments in applied magnetic fields. Then we establish that electric polarization is only allowed in the field-induced C structure, but not in the high-temperature IC and the zero-field C structures. Finally we show that the electric polarization is driven by the magnetic symmetry and propose a model that accounts for the temperature dependence of the ME constants.

Measurements were performed on a high-quality 0.4 g single crystal. Zero-field measurements were performed in a closed cycle cryostat on a four-circle goniometer at the TriCS single-crystal diffractometer, using neutron wavelength $\lambda=1.18$ Å for the C structure determination at $T=5$ K, and $\lambda=2.318$ Å for the IC structure at $T=21$ K. For diffraction measurements on the triple-axis spectrometer RITA-II, the sample was mounted in a 15 T magnet with the vertical field along the crystallographic c axis. The (H,T) phase diagram was determined using neutrons with $\lambda=4.04$ Å. The high-field magnetic structure was studied with $\lambda=2.02$ Å neutrons.

Symmetry properties. $LiNiPO_4$ crystallizes in the orthorhombic *Pnma* (No. 62) crystal structure with lattice parameters $a=10.02$ Å, $b=5.83$ Å, and $c=4.66$ Å.[17] The magnetic Ni^{2+} ions with spin $S=1$ are situated on $4(c)$ sites forming buckled planes perpendicular to the a axis. The positions of the four Ni^{2+} in each unit cell are $\mathbf{r}_1=(0.275,0.25,0.98)$, $\mathbf{r}_2=(0.775,0.25,0.52)$, $\mathbf{r}_3=(0.725,0.75,0.02)$, and $\mathbf{r}_4=(0.225,0.75,0.48)$, as shown in Fig. 1(a). The low crystal-field symmetry in $LiNiPO_4$ leads to a magnetic-susceptibility tensor that contains staggered off-diagonal terms, χ_{ac} and χ_{ca}. This allows for a single-ion anisotropy of the type

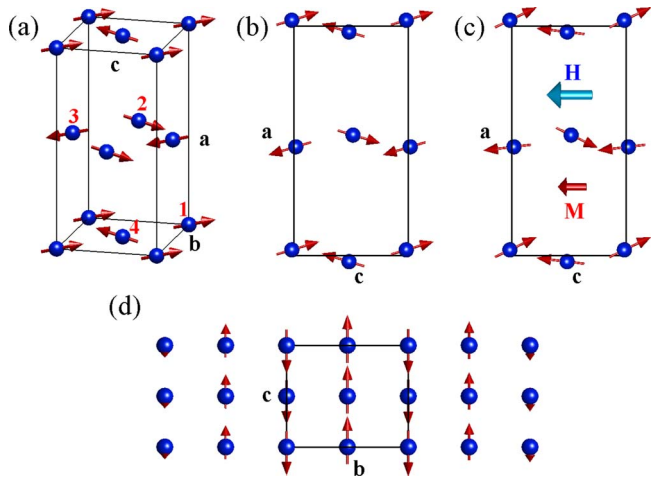

FIG. 1. (Color online) (a) Ni^{2+}-spin configuration of the zero-field C structure. Ni positions are labeled i according to their positions $\mathbf{r_i}$ ($i=1,\ldots,4$) but shifted $(-0.25,-0.25,0)$ compared to the values given in the text. [(b) and (c)] Projected C structure at zero and finite field $\mathbf{H}\|\mathbf{c}$ seen along the b axis. Spin angles are exaggerated for clarity. The applied field causes the Ni^{2+} moments to rotate, resulting in a magnetization $\mathbf{M}$ of the crystal, as described in the text. (d) Linearly polarized (LP) IC magnetic structure at zero field seen along the a axis.

$$\mathcal{H}_{zx}^{\mathrm{ani}} = -D_{zx}(S_1^c S_1^a - S_2^c S_2^a + S_3^c S_3^a - S_4^c S_4^a), \tag{1}$$

and two DM interactions

$$\mathcal{H}_1^{\mathrm{DM}} = D_1(S_1^c S_2^a - S_2^c S_1^a + S_3^c S_4^a - S_4^c S_3^a),$$

$$\mathcal{H}_2^{\mathrm{DM}} = -D_2(S_1^c S_4^a - S_4^c S_1^a - S_2^c S_3^a + S_3^c S_2^a). \tag{2}$$

Phase diagram. The (H,T) phase diagram for fields $\mathbf{H}\|\mathbf{c}$ up to $\mu_0 H=14.7$ T is shown in Fig. 2. The C phase is characterized by commensurate Bragg peaks associated with ordering vector $\mathbf{k}_C$, such as (0,1,0) whose T and H dependences are shown in Figs. 2(b) and 2(c). A sudden drop in intensity of the (0,1,0) peak indicates the collapse of the C phase in a first-order phase transition. Between $T=10$ and 18 K, the C phase extends to higher fields, leading to a dome-shaped (H,T) phase diagram. The C phase is enclosed by an IC phase with a magnetic ordering wave vector $\mathbf{k}_{IC}$, appearing, e.g., at $(0,1+q,0)$. Figures 3(a)–3(d) show the temperature dependence of q and the intensity of the IC $(0,1+q,0)$ peaks for different fields.

Staggered crystal fields and DM interactions. The zero-field C structure belongs to a single irreducible representation of $\mathbf{k}_C$, determined from 112 magnetic peaks at 5 K. The magnetic moments are nearly parallel to the c axis with $\mathbf{m}_C=(0.3(1),0,2.2(2))\mu_B$. The c component, m_C^c, has a $(+,+,-,-)$ order and the a component, m_C^a, has a $(+,-,-,+)$ order on the sites $\mathbf{r}_i$ with increasing $i=1,\ldots,4$ [Figs. 1(a) and 1(b)]. Earlier structural analysis using powder diffraction[18,19] found m_C^c, but not the smaller m_C^a. The presence of m_C^a may be explained by single-ion anisotropies and DM interactions. Inserting m_C^c of $(+,+,-,-)$ symmetry into Eqs. (1) and (2), we find that $\mathcal{H}_{zx}^{\mathrm{ani}}=-D_{zx}S(S_1^a-S_2^a-S_3^a+S_4^a)$ and $\mathcal{H}_{1,2}^{\mathrm{DM}}=-D_{1,2}S(S_1^a-S_2^a-S_3^a+S_4^a)$, which both favor that m_C^a is of $(+,-,-,+)$ symmetry.

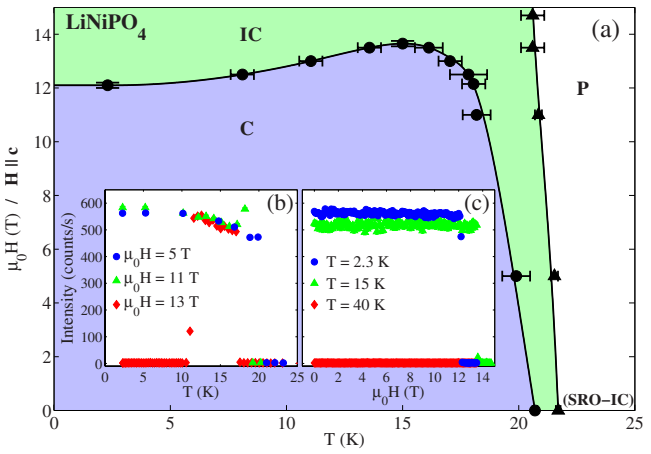

FIG. 2. (Color online) (a) (H,T) phase diagram of $LiNiPO_4$ for $\mathbf{H}\|\mathbf{c}$ including a C and an IC antiferromagnetic phase, and a paramagnetic (P) phase, which at zero field supports short-range fluctuations up to $T=40$ K (Ref. 13). [(b) and (c)] T and H dependences of the (0,1,0) magnetic Bragg peak intensity at three temperatures and fields.

Field-induced staggered moments. Magnetic fields along the c axis induce an antiferromagnetic (1,1,0) peak that grows as $(\mu_0 H)^2$ in the C phase [Fig. 3(e)]. High-energy (100 keV) x-ray diffraction at the BW5 beam line at HASYLAB, DESY, detected no field-dependent signal at (1,1,0), showing that the neutron signal is of magnetic origin. Structural refinements reveal that the (1,1,0) peak reflects an additional staggered magnetic a component, m_{st}^a, with $(+,-,+,-)$ symmetry, and an ordered moment increasing linearly with field to a value of $m_{st}\approx 0.17\mu_B$ at 12 T. Assuming that, to first order, the field rotates the magnetic moments without changing their magnitude, the magnetic structure [Fig. 1(c)] has a total ferromagnetic moment of $\sim(0,0,0.6m_{st}^a)$ per unit cell and the magnetization is $\mathbf{M}\approx(0,0,3.2)$ G at 12 T. This is consistent with bulk measurements[20] showing that the magnetization grows almost linearly with $\mathbf{H}$ and is ~ 0.03 G at 0.1 T. At 40 K, where the system is paramagnetic, there is still field-induced (1,1,0) intensity [Fig. 3(e)]. We interpret this as staggered magnetic fields at the Ni position due to off-diagonal elements of the local susceptibility tensor or the DM interactions, as previously observed in antiferromagnetic $S=\frac{1}{2}$ chains.[21,22]

The IC magnetic order at zero field is a transversely polarized collinear spin-density wave belonging to a single representation of $\mathbf{k}_{IC}$. The structure is shown in Fig. 1(d) and consists of magnetic moments $\mathbf{m}_{IC}=(0.0(2),0.0(1),1.2(2))\mu_B$ that are ordered with $(+,+,-\beta,-\beta)$ symmetry, where $\beta=e^{-i\pi q}$ describes the IC modulation along $\mathbf{b}$. The IC component of the high-field structure is found by structural analysis of 83 magnetic peaks at 14.7 T and 2.3 K. The best fit results in a similar structure as at zero field, but with increased amplitude $\mathbf{m}_{IC}=(0,0,2.0(2))\mu_B$. However, the data do not exclude an elliptically polarized (EP) IC structure with $(+,+,-\beta,-\beta)$ components along a and c. An EP IC structure at 14.7 T and 2.3 K is directly

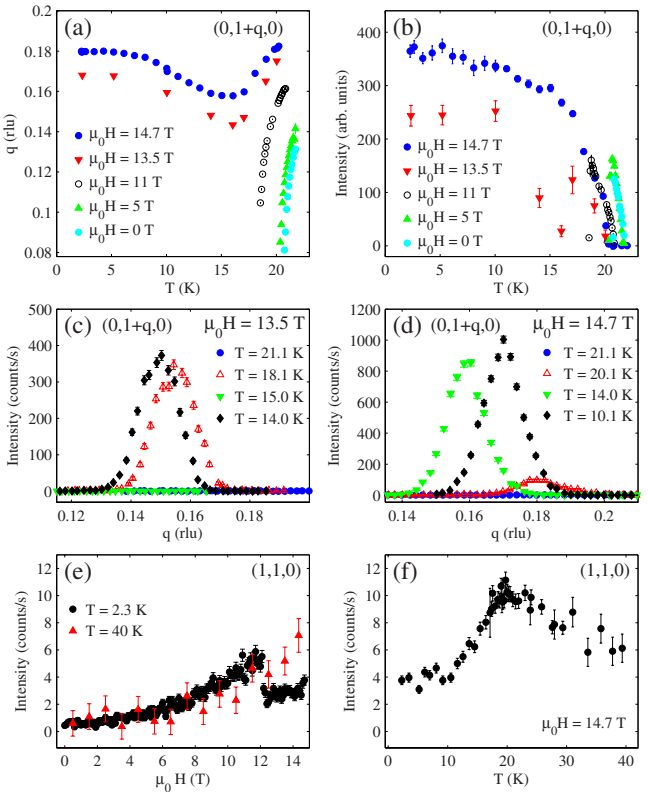

FIG. 3. (Color online) [(a) and (b)] Position and integrated intensity of the $(0,1+q,0)$ IC peak as function of temperature for different fields $\mathbf{H}\|\mathbf{c}$. [(c) and (d)] Scattering intensity for wave vectors $(0,k,0)$ at $\mu_0 H = 13.5$ and 14.7 T. At 13.5 T, the IC peak disappears near $T = 15$ K where the system enters the C phase [cf. Fig. 2(a)]. [(e) and (f)] Background-subtracted peak intensities of the (1,1,0) peak as function of field and temperature.

supported by analysis of higher-order harmonics and indirectly by a mean-field calculation predicting a phase boundary between the EP IC structure and a high-temperature linearly polarized (LP) IC structure around 15 K at 14.7 T.[23] Coexisting with the IC order is a field-induced (1,1,0) intensity [Figs. 3(e) and 3(f)] signaling a $(+,-,+,-)$ C-type moment along the a axis of approximately $0.11\mu_B$.

Phenomenology. The zero-field C structure breaks inversion symmetry, but is invariant under 2_b (180° screw axis along **b**), thus preventing electric polarization perpendicular to **b**. However, for $\mathbf{H}\|\mathbf{c}$ the invariance under 2_b is broken and electric polarization is allowed. The LP IC structures leave at least one point of inversion invariant and do not allow for electric polarization—even in the presence of the C staggered moments. This is consistent with a more formal treatment developed by Harris.[24]

Magnetoelectric effect. The main features of the ME effect in $LiNiPO_4$ can be explained by connections between superexchange (SE), DM spin interactions, and elastic distortions. At zero field $|\mathbf{S}_1| = |\mathbf{S}_2| = |\mathbf{S}_3| = |\mathbf{S}_4| = \langle S \rangle$, the thermal mean value of the spin operator, and the angles between $\mathbf{S}_1$ and $\mathbf{S}_2$ and between $\mathbf{S}_3$ and $\mathbf{S}_4$ are identical, $\theta_{12} = \theta_{34} = \theta$. In the C phase a magnetic field $\mathbf{H}\|\mathbf{c}$ rotates the spins as shown in Fig. 4(c). Here $\theta_{12} = \theta + \Delta\theta$ and $\theta_{34} = \theta - \Delta\theta$, and $\Delta\theta$ is proportional to the magnetization $\chi_c H_z$, if we assume that

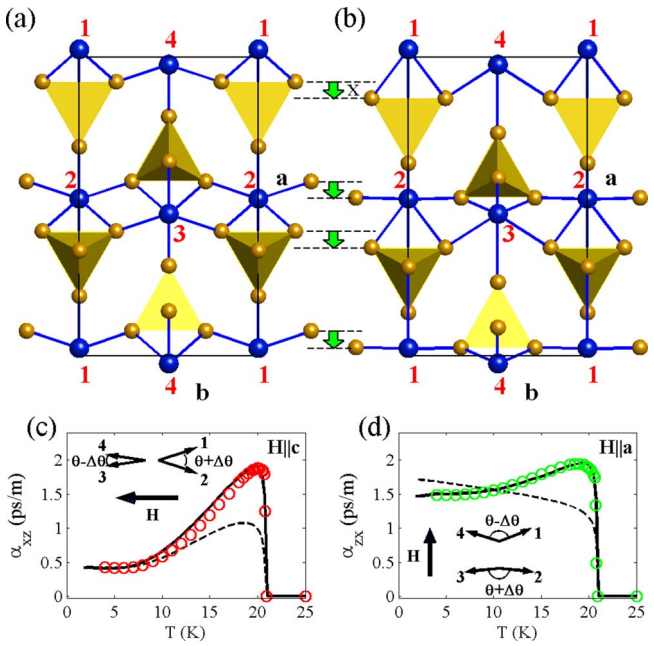

FIG. 4. (Color online) (a) Positions of Ni [large blue (dark) circles], O [small yellow (bright) circles], and the PO_4 tetrahedra (triangles) in zero field. (b) Same as (a), but for $\mathbf{H}\|\mathbf{c}$. PO_4 tetrahedra are assumed to shift downward with x (arrows), giving an electric polarization P_x and changing the SE interaction as explained in the text. (c) Measured (circles) (Ref. 13) and calculated ME coefficients α_{xz} for $\mathbf{H}\|\mathbf{c}$, assuming identical spin lengths (dashed line) and different spin lengths (solid line). (d) Same as (c) for α_{zx} with $\mathbf{H}\|\mathbf{a}$. Insets of (c) and (d) show the assumed angles between $\mathbf{S}_1$, $\mathbf{S}_2$, $\mathbf{S}_3$, and $\mathbf{S}_4$.

$|\mathbf{S}_1| = |\mathbf{S}_2| = |\mathbf{S}_3| = |\mathbf{S}_4|$ even at nonzero fields. The SE energy for $\mathcal{H}^{\mathrm{SE}}_{12,34} = J_{12}\mathbf{S}_1 \cdot \mathbf{S}_2 + J_{34}\mathbf{S}_3 \cdot \mathbf{S}_4$ in this spin configuration is

$$\mathcal{E}^{\mathrm{SE}}_{12,34} = (J_{12} + J_{34})\langle S \rangle^2 \left(1 - \frac{1}{2}(\theta^2 + \Delta\theta^2)\right) - (J_{12} - J_{34})\langle S \rangle^2 \theta \Delta\theta. \quad (3)$$

SE energy (3) can be lowered by a uniform displacement of exchange mediating ions such as the translation of all PO_4 tetrahedra along **a** by a small distance x [Fig. 4(b)]. The symmetry of the Ni-O-P-O-Ni exchange paths implies that a uniform translation of the tetrahedra, leading to an electric polarization P_x along **a**, simultaneously increases J_{12} and reduces J_{34}, or vice versa. To first order $J_{12} = J + \delta$ and $J_{34} = J - \delta$, where $\delta = \lambda_x x$ for small values of x. Introducing an elastic energy $\epsilon_x x^2$ for the tetrahedra displacements gives a SE-elastic interaction energy $-2\lambda_x \langle S \rangle^2 \theta \Delta\theta x + \epsilon_x x^2$, which is minimum for $x = \lambda_x \langle S \rangle^2 \theta \Delta\theta \epsilon_x^{-1}$. Noting that $P_x \propto x$ and $\Delta\theta \propto \chi_c H_z$ we obtain an electrical polarization $P_x \propto \epsilon_x^{-1} \langle S \rangle^2 \chi_c H_z$, and thereby a ME coefficient $\alpha_{xz} \propto \epsilon_x^{-1} \langle S \rangle^2 \chi_c$. An equivalent expression for α_{xz} can also be obtained from the DM interaction term H_1^{DM}. These ME coefficients are similar to the phenomenological expressions suggested by Rado[25] but are here established from a microscopic point of view related to Ref. 11. Figure 4(c) compares the temperature dependence of the measured ME coefficient α_{xz} (Ref. 13) to $\epsilon_x^{-1} \langle S \rangle^2 \chi_c$

(dashed line), assuming a constant elastic coefficient ϵ_x and using the magnetic order parameter $\langle S\rangle$ determined in Ref. 19 and the magnetic susceptibility χ_c from Refs. 20 and 26. A more elaborate calculation of α_{xz}, assuming the angle difference $\Delta\theta$ fixed at the low-temperature value, while the spins have nonidentical lengths at finite temperatures, gives significantly better agreement with the experimental data [solid line in Fig. 4(c)]. Here the expressions for SE and DM are not equivalent and both terms are needed in the best fit to the data.

To explain the elastic distortions in the C phase for $\mathbf{H}\|\mathbf{a}$ we first assume, as for $\mathbf{H}\|\mathbf{c}$, that the magnetization of the sample results from a rotation of the magnetic moments. This way we obtain the C spin structure sketched in Fig. 4(d). Using similar arguments, now on the pairs $(\mathbf{S}_1,\mathbf{S}_4)$ and $(\mathbf{S}_2,\mathbf{S}_3)$, we find for identical spin lengths a ME coefficient $\alpha_{zx}\propto\epsilon_z^{-1}\langle S\rangle^2\chi_a$ (dashed line), which is compared to the measured ME coefficient α_{zx} (Ref. 13) in Fig. 4(d). Once again the elaborate calculation (solid line) improves the agreement with the experimental data.

The proposed mechanism for ME distortions is not effective for $\mathbf{H}\|\mathbf{b}$ in the C phase, nor for any field direction in the LP IC phase. In the former case, all spins will cant with the same amount in the field direction and have the same lengths, leading to no energy differences between any pairs of spins and no magnetoelectricity. In the LP IC case, the observed spin structures are superpositions of C and IC components, which are uncoupled in the energy terms because of translational symmetry. The symmetries of the C and the IC components considered separately do not produce the needed energy differences and ME distortions are therefore not induced.

Conclusions. The symmetries of the established magnetic structures do not support an electric polarization in the C and zero-field IC phases. Applying a magnetic field along **c** in the C phase creates a polar axis and allows for electric polarization. Symmetry analysis show that electric polarization is possible in the C phase structure, but not in the LP IC phase. A microscopic model explains the temperature dependence of the ME constants, providing evidence that the electric polarization in $LiNiPO_4$ results from field-induced changes in the magnetic structure.

Jens Jensen is greatly acknowledged for illuminating discussions. Work was supported by the Danish Agency for Science, Technology and Innovation under DANSCATT and by the Swiss National Science Foundation via Contracts No. PP002-102831 and No. 200020-105175. This Brief Report was authored, in whole or in part, under Contract No. DE-AC02-07CH11358 with the U.S. Department of Energy. This research project is based on experiments performed at the Swiss spallation neutron source SINQ, Paul Scherrer Institute, Villigen, Switzerland.

[1] M. Fiebig, J. Phys. D **38**, R123 (2005).
[2] D. I. Khomskii, J. Magn. Magn. Mater. **306**, 1 (2006).
[3] S. W. Cheong and M. Mostovoy, Nature Mater. **6**, 13 (2007).
[4] M. Kenzelmann, G. Lawes, A. B. Harris, G. Gasparovic, C. Broholm, A. P. Ramirez, G. A. Jorge, M. Jaime, S. Park, Q. Huang, A. Ya. Shapiro, and L. A. Demianets, Phys. Rev. Lett. **98**, 267205 (2007).
[5] A. Pimenov, A. A. Mukhin, V. Yu. Ivanov, V. D. Travkin, A. M. Balbashov, and A. Loidl, Nat. Phys. **2**, 97 (2006).
[6] A. B. Sushkov, R. V. Aguilar, S. Park, S. W. Cheong, and H. D. Drew, Phys. Rev. Lett. **98**, 027202 (2007).
[7] T. Kimura, T. Goto, H. Shintani, K. Ishizaka, T. Arima, and Y. Tokura, Nature (London) **426**, 55 (2003).
[8] G. Lawes, A. B. Harris, T. Kimura, N. Rogado, R. J. Cava, A. Aharony, O. Entin-Wohlman, T. Yildrim, M. Kenzelmann, C. Broholm, and A. P. Ramirez, Phys. Rev. Lett. **95**, 087205 (2005).
[9] M. Kenzelmann, A. B. Harris, S. Jonas, C. Broholm, J. Schefer, S. B. Kim, C. L. Zhang, S.-W. Cheong, O. P. Vajk, and J. W. Lynn, Phys. Rev. Lett. **95**, 087206 (2005).
[10] M. Mercier, Ph.D. thesis, Université de Grenoble, 1969.
[11] R. Hornreich and S. Shtrikman, Phys. Rev. **161**, 506 (1967).
[12] I. A. Sergienko and E. Dagotto, Phys. Rev. B **73**, 094434 (2006).
[13] D. Vaknin, J. L. Zarestky, J.-P. Rivera, and H. Schmid, Phys. Rev. Lett. **92**, 207201 (2004).
[14] V. M. Khrustalyov, V. N. Savitsky, and N. F. Kharchenko, Czech. J. Phys. **54**, 27 (2004).
[15] I. Kornev, M. Bichurin, J.-P. Rivera, S. Gentil, H. Schmid, A. G. M. Jansen, and P. Wyder, Phys. Rev. B **62**, 12247 (2000).
[16] I. E. Chupis, Low Temp. Phys. **26**, 419 (2000).
[17] I. Abrahams and K. S. Easson, Acta Crystallogr., Sect. C: Cryst. Struct. Commun. **49**, 925 (1993).
[18] R. P. Santoro, D. J. Segal, and R. E. Newnham, J. Phys. Chem. Solids **27**, 1192 (1966).
[19] D. Vaknin, J. L. Zarestky, J. E. Ostenson, B. C. Chakoumakos, A. Goñi, P. J. Pagliuso, T. Rojo, and G. E. Barberis, Phys. Rev. B **60**, 1100 (1999).
[20] Yu. N. Kharchenko, N. F. Kharcheno, M. Baran, and R. Szymczak, Low Temp. Phys. **29**, 579 (2003).
[21] M. Oshikawa and I. Affleck, Phys. Rev. Lett. **79**, 2883 (1997).
[22] Y. Chen, M. B. Stone, M. Kenzelmann, C. D. Batista, D. H. Reich, and C. Broholm, Phys. Rev. B **75**, 214409 (2007).
[23] J. Jensen (private communication).
[24] A. B. Harris, Phys. Rev. B **76**, 054447 (2007).
[25] G. T. Rado, Phys. Rev. Lett. **6**, 609 (1961).
[26] J. Li and D. Vaknin (unpublished).